Journal of Materials Chemistry A

PAPER

Cite this: J. Mater. Chem. A, 2017, 5, 11009

In situ formation of highly active Ni–Fe based oxygen-evolving electrocatalysts *via* simple reactive dip-coating†

Guofa Dong,‡[abc] Ming Fang,‡[ad] Jianshuo Zhang,[c] Renjie Wei,[ad] Lei Shu,[ad] Xiaoguang Liang,[ad] SenPo Yip,[ad] Fengyun Wang,[e] Lunhui Guan,[c] Zijian Zheng*[b] and Johnny C. Ho*[adf]

Received 6th February 2017
Accepted 26th April 2017

DOI: 10.1039/c7ta01134b

rsc.li/materials-a

Since the oxygen evolution reaction (OER) is a key step in the process of water splitting, efficient catalysts are inevitably required to overcome energy barriers at the electrode–electrolyte interface in order to improve its reaction efficiency; as a result, developing highly active and low-cost catalysts is of the great importance. Herein, we report an extremely simple method to prepare OER catalysts, which exhibit excellent activity and superior OER stability in alkaline conditions. The OER catalysts are composed of mixed Ni–Fe oxides or hydroxides that can be easily obtained by *in situ* reactive dip-coating of nickel foams in a Fe^{3+}-containing aqueous solution. In specific, the as-prepared composites can give an overpotential value of 210 mV under a current density of 10 mA cm^{-2} in 1 M KOH aqueous solution and there is not any obvious degradation in OER activity even after 50 hour's chronopotentiometry measurement at a current density of 50 mA cm^{-2}. More importantly, the samples prepared by this method also illustrate the good uniformity, in which this particular synthesis scheme would hold the great potency for practical fabrication of high-performance and low-cost catalysts in the large-scale industrialization.

1. Introduction

Nowadays, hydrogen is widely considered as a promising green fuel to relieve the energy crisis as well as to reduce the adverse environmental impact of the fossil fuel utilization.[1,2] Among a variety of methods of producing hydrogen, water electrolysis, which can be driven by any intermittent and renewable energy resources, such as solar energy, wind power, tidal energy, *etc.*, is an appealing approach to obtain highly pure hydrogen economically and environment-friendly. In general, there are two half-reactions in the overall water electrolysis, namely hydrogen evolution reaction (HER) and oxygen evolution reaction (OER). Theoretically, this hydrogen production scheme can be implemented with an efficiency of 100% without the release of any pollutant during the water splitting process.[3,4] However, as compared with the HER, the OER is a kinetically sluggish process since multiple reaction steps are involved;[5,6] therefore, the ultimate efficiency would always get degraded. In this regard, exploiting and developing high-performance and cost-effective OER electrocatalysts is of the great importance to achieve the highly efficient water splitting in order to realize the above-mentioned hydrogen energy scheme and to benefit our society. Although noble metal oxides, such as RuO_2 and IrO_2, are excellent OER catalysts,[7,8] they cannot meet the huge demand for the future large-scale hydrogen production due to their high price and extreme scarcity on the earth. In recent years, various earth-abundant OER catalysts have been extensively exploited and developed.[8,9] Among these alternatives, 3d transition metals, including Fe, Co, Ni, Mn, and their oxides, (oxy)hydroxides, chalcogenides, phosphates or borides, have shown great promise by offering high activities and excellent stabilities in the OER.[10–20] In particular, several Fe-containing Co- and Ni-(oxy)hydroxides demonstrate even better catalytic performances than those of the state-of-the-art precious counterparts, such as RuO_2 and IrO_2.[18–20] Nevertheless, in addition to the material cost, the manufacturing cost should also be considered as an important factor for the large-scale utilization of these catalysts. Even though there are many different production methods, involving electrochemical

[a]Department of Physics and Materials Science, City University of Hong Kong, Kowloon Tong, Kowloon, Hong Kong SAR, P. R. China. E-mail: johnnyho@cityu.edu.hk
[b]Nanotechnology Center, Institute of Textiles and Clothing, The Hong Kong Polytechnic University, Hung Hom, Kowloon, Hong Kong SAR, P. R. China. E-mail: tczzheng@polyu.edu.hk
[c]Key Laboratory of Design and Assembly of Functional Nanostructures, Fujian Institute of Research on the Structure of Matter, Chinese Academy of Sciences, Fuzhou 350108, P. R. China
[d]Shenzhen Research Institute, City University of Hong Kong, Shenzhen 518057, P. R. China
[e]Cultivation Base for State Key Laboratory, Qingdao University, Qingdao 266071, P. R. China
[f]State Key Laboratory of Millimeter Waves, City University of Hong Kong, Kowloon Tong, Kowloon, Hong Kong SAR, P. R. China

† Electronic supplementary information (ESI) available. See DOI: 10.1039/c7ta01134b

‡ These authors contributed equally.

deposition,[11,21,22] hydrothermal,[23–25] spin-coating,[18,26] vapor deposition,[14] photochemical processes[27] and such, have been established and employed to fabricate these OER catalysts, major of these fabrication schemes still suffer from the relatively complicated operation, which often requires expensive equipment for the scalable production. As a result, in order to make the water electrolysis as an economically competitive choice for the hydrogen generation, extremely simple fabrication methods should be developed for high-performance and low-cost OER catalysts.

In this work, we propose, establish and demonstrate an exceptionally simple scheme to prepare OER catalysts, which illustrate excellent activity and superior OER stability in alkaline conditions. The OER catalysts are composed of Ni–Fe based composites that can be easily obtained by *in situ* reactive dip-coating of nickel foams in a Fe^{3+}-containing aqueous solution. Even though this catalyst production method only utilizes low-cost precursor materials with the fabrication process completed in just a few minutes, the obtained catalysts exhibit impressively high electrocatalytic OER activity, which is even much better than those of precious OER catalyst materials, including the well-known high-performance RuO_2 nanoparticles. More importantly, the catalysts are also demonstrated with excellent stability without any obvious performance decay over 50 hour's chronopotentiometry measurement at a current density of 50 mA cm^{-2}. All these have evidently indicated the great potency of these cost-effective catalysts for practical utilizations in the large-scale industrialization.

2. Experimental section

2.1. Materials

Nickel foams (NFs) with a thickness of 1.05 mm and a bulk density of 0.30 g cm^{-3} (CORUN, Ltd., Changsha, China) were used as the substrate. Iron(III) chloride ($FeCl_3$, anhydrous, 99+%, GR) was purchased from International Laboratory USA while hydrochloric acid (HCl, ACS regent, 37%), ethanol absolute and isopropanol alcohol (ACS reagent, 99.5+%) were purchased from Sigma-Aldrich. Potassium hydroxide (KOH, 95%) was from Shanghai Meryer Chemical Technology Co. Ltd. and RuO_2 nanoparticles with an average size of less than 10 nm were obtained from China Rare Metal Material Co. Ltd. All the aqueous solutions were prepared with Milli-Q water with the resistance of 18.2 MΩ cm at 25 °C.

2.2. Dip-coating of NiFe composites onto Ni foams

NFs were first cut into sheets with a size of 8 × 30 mm and sonicated in HCl solution (1 M) for 10 minutes to remove the surface oxide layer followed by rinsing with water and ethanol absolute, sequentially. The NF sheets were next blow-dried with the nitrogen gas. As depicted in Fig. 1, the cleaned NF sheets were then dipped into 50 mM $FeCl_3$ aqueous solutions and kept for 10 seconds, then taken out and annealed on a hot plate. The temperature of the hotplate was set at 300 °C and the annealing time was 30 minutes. The finished NF sheets were then denoted as NiFeOH@NF.

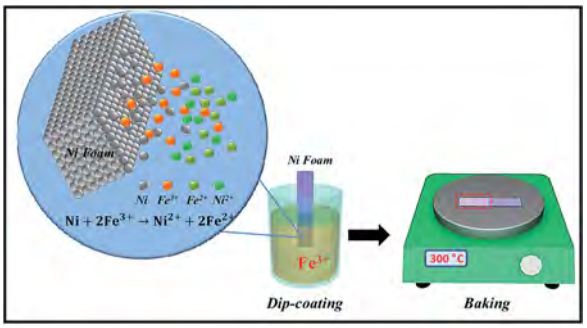

Fig. 1 Schematic illustration of the reactive dip-coating process with the reaction process given in the inset.

2.3. Fabrication of the NiFeOH@NF electrode and NF electrode

In order to get a fixed geometric electrode area for the electrochemical measurement, the fabricated NiFeOH@NF samples were sealed with a silicone rubber which is insulating and chemically stable. After that, the length of 10 mm was left and the total geometric electrode area counted on both sides is 1.6 cm^2. As a control, a bare NF electrode with the same size was also prepared.

2.4. Preparation of the RuO_2@glass carbon electrode (GCE)

Commercial RuO_2 powders are often used as standard catalysts for the OER.[24,28,29] Here, for the explicit performance comparison, RuO_2 powder was also loaded on a mirror polished GCE (5 mm in diameter). 20 μL dispersion of RuO_2 nanoparticles (2 mg mL^{-1} in isopropanol alcohol with 0.1% v/v Nafion) was then drop-coated onto the GCE surface and dried in open air under an infrared lamp. The loading weight was controlled and estimated as 0.2 mg cm^{-2}. The details can be found in the ESI.†

2.5. Physical characterization

Scanning electron microscopy (SEM) imaging and elemental mapping were performed on a Zeiss Merlin Compact with an Oxford X-50 max energy dispersive spectrometer (EDS) system (Oxford Instruments) operated at 10 kV. EDS was determined on an environmental scanning electron microscope (FEI/Philips XL30 ESEM-FEG, Finland) system. Transmission electron microscopy (TEM) images were obtained from Tecnai G2-F30 (FEI, US) operated at 200 kV. In particular, samples were prepared by vigorously sonicating the NiFeOH@NF sample in ethanol absolute and drop casting the ethanol dispersion onto copper grids. X-ray photoelectron spectroscopy (XPS) was carried out on a Thermo Scientific ESCALAB 250Xi X-ray photoelectron spectrometer. The XPS data were analyzed and fitted with XPSPEAK 4.1 software.

2.6. Electrochemical characterization

All electrochemical measurements were carried out using a G-300 electrochemical workstation (Gamry Instruments) connected with a standard three-electrode configuration under

a room temperature of 25 °C. The fabricated NiFeOH@NF sample was used as the working electrode. A saturated calomel electrode (SCE) and a Pt wire were employed as the reference electrode and counter electrode, respectively. All potentials reported in this work were calibrated *versus* the reversible hydrogen electrode (RHE) using the equation: $E_{RHE} = E_{SCE} + (0.242 + 0.059 \times pH)V$, where E_{RHE} is the potential referred to the RHE and E_{SCE} is the measured potential against the SCE reference electrode. The OER activity was surveyed by cyclic voltammetry (CV) at a scan rate of 5 mV s^{-1}. To keep the electrode surface in a relatively stable state, 10 CV cycles were operated before the assessment of OER activity until the redox peaks and the oxygen evolution currents showed any unobvious change. The overpotential values corresponding to different current densities were determined from the cathodic-going half cycle of the CV curves. Unless specifically mentioned, the voltammograms were recorded with *iR* drop compensation automatically on the workstation. The OER stability was determined by chronopotentiometry measurements at a current density of 50 mA cm^{-2} without any *iR* drop compensation.

2.7. Evaluation of the electrochemical surface area (ECSA)

The ECSA of NF-based electrodes were estimated by the electrochemical double-layer capacitance method as previously reported.[30,31] The capacitance of the catalytic surface was measured from the non-faradaic capacitive current associated with double-layer charging from the scan-rate dependence of cyclic voltammograms (CVs). Cyclic voltammograms were recorded in a non-faradaic region (−0.050 to 0.050 V *vs.* SCE) at the following scan rate: 10, 25, 50, 100, 200, 400, and 600 mV s^{-1}. More details are provided in the ESI.†

3. Results and discussion

The electrode reaction is essentially an interface process occurring between the electrode surface and the bulk solution, and the properties of the surface layer of the electrode catalyst can fundamentally determine the catalytic performance. As reported before, the OER activity of the Ni compounds can be greatly enhanced even by a trace amount of Fe incorporating into the Ni oxides or hydroxide.[19,32] In this work, based on a common oxidation reaction between Fe^{3+} ions and Ni metal atoms, we design and employ a simple reactive dip-coating scheme to combine Fe species into the surface layer of Ni foams. This way, the Ni–Fe catalyst layer can be *in situ* formed in a fast and straight-forward way while the skeleton of Ni foams can also be well maintained to enable the stable framework for sufficient reactive surface area and electron transport paths for the enhanced OER performance. The successful *in situ* growth of the NiFe compound on Ni foam was proved by the apparent difference of the nickel foam color, as shown in Fig. S1.† The bare Ni foam was initially silvery grey while the color was turned into light brown after the dip-coating process. In particular, as illustrated in Fig. 2a and b and S1,† the morphology of NF and NiFeOH@NF was observed under SEM. It is found that before dip-coating, the pure Ni foam was very clean and the Ni metal

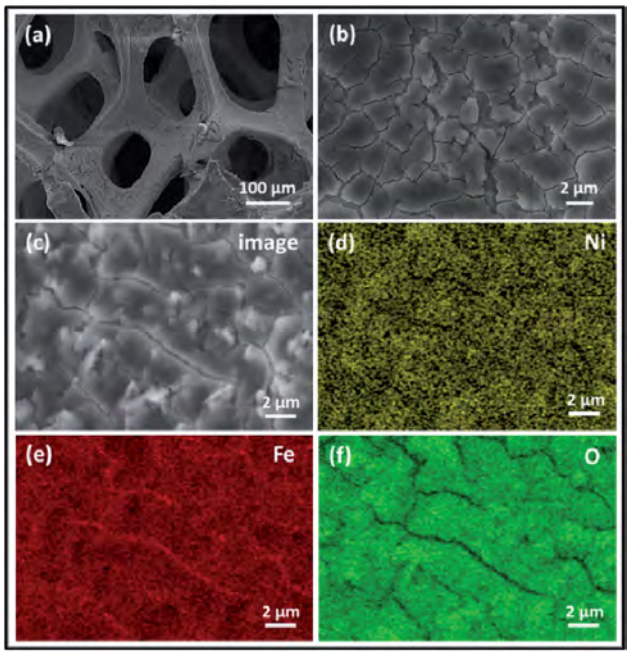

Fig. 2 (a and b) SEM images of NiFeOH@NF and (c–f) the elemental mapping images for Ni (yellow), Fe (red) and O (green) of the NiFeOH@NF sample.

grains can be seen clearly with the grain sizes of about 10 μm (Fig. S1a and c†), while after the reactive dip-coating, the NF surface became much rougher and many island-like features with the size of several micrometers were formed on the grain surface (Fig. S1b and d†). To analyze the surface chemical compositions and their element distributions, EDS characterization was first employed on the as-produced NiFeO@NF (Fig. S2 and Table S1†). The EDS result gave a relatively low atomic Fe/Ni ratio, and such a high Ni signal may have arisen from the background contribution of the nickel foam. In order to rule out the information from Ni foams, the EDS spectra were then recorded for the clusters directly stripped off from the surface coatings, which gave a much higher Fe/Ni atomic ratio. Obviously the Ni element in the NiFeO@NF was from the Ni foam etched by the oxidation reaction between the surface Ni atoms and the Fe^{3+} in the solution. According to the EDS results from different detection modes, the surface coatings are found to be mainly composed of Ni, Fe and O, and the Fe/Ni atomic ratio varied at different detected spots. In any case, based on the EDS mapping as shown in Fig. 2c–f, all constituents are uniformly distributed, indicating that the element distribution are relatively uniform at the sample surface in the long-range order. The discrepancy between the spot detection and the mapping can be probably attributed to the variation of the Fe/Ni atomic ratio along the depth direction. To further assess the distributions of Ni, Fe and O, elemental mapping was performed along the cross-section of the sample and the results were analyzed (Fig. S3†). It showed that the intensity of Ni signal in the skeleton of Ni foam was more intense than that in the surface layer, while the signals of Fe and O could only be found in the surface layer and their distributions existed in the uneven

state, which may be resulting from the heterogeneous reactions of the dip-coating process. From the above-mentioned results, it is clear that the reactive dip-coating method can successfully accomplish Fe incorporation into the NFs and greatly modify their surface morphology, which may be favorable to acquire high-performance OER catalysts.

Moreover, TEM was employed to evaluate the morphology and crystallinity of the fabricated NiFeOH compounds. As shown in Fig. 3, the as-obtained compounds were composed of randomly orientated nanocrystals with the size of a few nanometers. Unfortunately, due to the overlapping of these nanocrystals, it is difficult to retrieve any conclusive crystalline information from the lattice fringes. Therefore, we turned to utilize SAED to analyze the phases of the fabricated layer. The SAED pattern of the sample showed diffused rings, indicating that the material was composed of nearly amorphous phases or small nanocrystals, which was consistent with the HRTEM results. By measuring the radius (R) of the diffraction rings, the d-space between the crystal planes was obtained by $d = 1/R$. It was found that the obtained d values match well with the lattice information of Goethite FeOOH crystals (ref. PDF#29-0713). The details on the analysis of SAED were given in Fig. S4 and Table S2 in the ESI.† However, such a unique polycrystalline structure can provide plenty of lattice defects and thus more exposure of low-coordinated surface atoms. Previous reports showed that defect points in the catalysts often gave birth to the active sites because of the rich dangling bonds.[33–35] In order to further investigate the surface composition and corresponding chemical states, the NiFe compounds were then examined thoroughly by XPS. It is evident in Fig. 4a that the spectra reveal the presence of Ni, Fe and O of the sample, which is consistent with the EDS results. Notably, as illustrated in Fig. 4b, the high-resolution Ni $2p_{3/2}$ spectrum can be deconvoluted into 5 distinct characteristic peaks. Those 4 peaks towards the low energy region at 852.7, 853.9, 855.7 and 857.4 eV correspond to Ni^0, NiO, $Ni(OH)_2$, and NiOOH, respectively, while the high energy peak at 861.8 eV represents the shake-up satellite peak of the Ni $2p_{3/2}$ level.[36,37] The fitting peaks of Ni $2p_{1/2}$ at 871.9, 873.8 and 880.1 eV were indexed to Ni^{2+}, Ni^{3+} and shake-up peak of Ni $2p_{1/2}$, respectively.[38,39] As compared to the Ni 2p spectrum, the Fe 2p spectrum is relatively complicated, including much more complex chemical information of Fe^{2+} and Fe^{3+}. For instance, the XPS data of Fe oxides, hydroxides and oxyhydroxides have been widely investigated by many researchers,[40–43] but there is still not any common standard established due to the involvement of many different complex factors, such as the chemical environment, the conditions of XPS measurement and even the synthetic method of the samples. In this case, we refer to the most approximate peak values in order to analyze the Fe 2p spectrum in Fig. 4c. It is found that both Fe^{3+}- and Fe^{2+}-containing compounds are existed in the sample. In specific, the peaks at 709.9 and 711.6 eV correspond to Fe^{2+} $2p_{3/2}$ and Fe^{3+} $2p_{3/2}$, accordingly, accompanied by their satellite peaks at 715.3 and 719.4 eV. More detailed peak attribution is also listed in Table S3 of the ESI.† More importantly, based on the O 1s spectrum as depicted in Fig. 4d, there are several oxygen-containing species existed in the NiFeOH@NF sample here.[42,44] The three peaks at 530.1, 531.6 and 533.2 eV can be attributed to the contributions from the lattice of oxides, hydroxides and absorbed water,[44] respectively. All these results evidently indicate that both NiFe oxides and hydroxides are formed in the surface layer coatings.

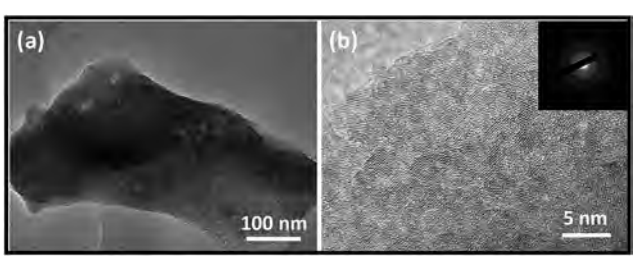

Fig. 3 (a) Typical TEM and (b) HRTEM images of surface layer of the as-obtained NiFeOH@NF. The inset in (b) is the SAED pattern.

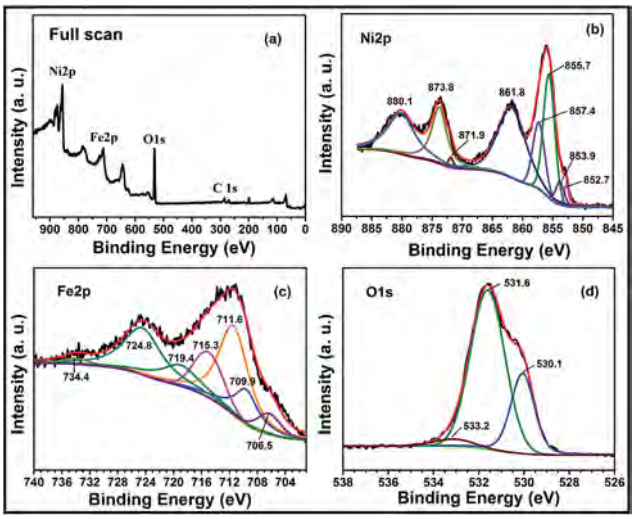

Fig. 4 (a) X-ray photoelectron survey spectrum, (b) Ni 2p, (c) Fe 2p and (d) O 1s spectra of the NiFeOH@NF sample.

To shed light on the corresponding OER performance, the electrocatalytic activity of the Ni foam, NiFeOH@NF and commercial RuO_2 nanoparticle loaded sample were evaluated in the alkaline solution (1 M KOH) with a standard three-electrode system. Cyclic voltammograms were recorded from 0 to 0.6 V *vs.* the SCE and the scan rate was 5 mV s^{-1}. As shown in the CV plot in Fig. 5a, the cathodic-going half cycles were used to determine the OER activity to avoid the interference from the oxidation peak of Ni^{2+} to Ni^{3+} at about 1.35–1.45 V *vs.* the RHE.[30] It is obvious that before the reactive dip-coating, the Ni foam exhibited poor activity towards the OER; however, after the dip-coating, the OER activity of the NiFeOH@NF sample was greatly improved, even much better than that of the one loaded with the commercial RuO_2 nanoparticles, which are well known for excellent OER performance. In order to obtain a current density of 10 mA cm^{-2}, the overpotential values on RuO_2 nanoparticles and Ni foam were 275 mV and 374 mV, respectively, while the overpotential on NiFeOH@NF was just 210 mV. More OER

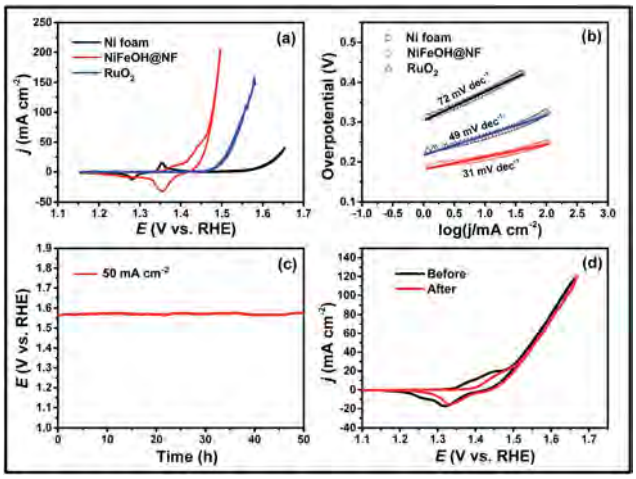

Fig. 5 (a) CV plots of the OER process performed on the Ni foam, NiFeOH@NF and glass carbon electrode loaded with the commercial RuO_2 nanoparticles in 1 M KOH with a scan rate of 5 mV s^{-1}; (b) the corresponding Tafel slopes on the Ni foam, NiFeO@NF and RuO_2 nanoparticle loaded sample; (c) chronopotentiometry plot of the OER process operated with the NiFeOH@NF sample under a current density of 50 mA cm^{-2}; (d) CV curves for the OER process before and after the chronopotentiometry measurement with the duration of 50 h. Note that all the CV curves in (a) were recorded under IR compensation mode and the curves in the (c) and (d) were collected without the *iR* compensation.

overpotential values (η) under different current densities (j) with different catalyst materials were as well listed in Table 1. Explicitly, the NiFeOH@NF sample showed the best OER catalytic activity among these three materials, especially under the high current densities. It is clear that the reactive dip-coating method can be used to fabricate NiFeOH@NF with improved OER activity.

Generally, Tafel slopes are an important parameter to estimate the performance of an OER catalyst. It manifests how the current density changes with increasing overpotential values and contains important information about the reaction mechanism.[45] In this work, Tafel slopes on different catalyst materials were also analyzed and are illustrated in Fig. 5b. The NiFeOH@NF sample gave a Tafel slope of 31 mV dec^{-1}, while the ones of the NF and RuO_2 nanoparticle loaded specimen were 72 and 49 mV dec^{-1}, respectively. This excellent electrocatalytic OER activity of NiFeOH@NF also suggests one of the best results reported in the recent literature studies (Table S4†), in which this good catalytic performance can be attributed to the rich chemical content, diverse structures and various valence states of Ni and Fe of the NiFeOH layer. As reported in other studies, the Ni metal and Ni oxides are often used as anode materials for the OER in industries under alkaline conditions because of their low material cost and good stability.[46,47] With the introduction of Fe, the Ni oxides could get significantly improved in their electrocatalytic OER activity.[32] In specific, the OER activities of Ni–Fe films with a composition of 40 atomic% Fe were roughly 2 orders of magnitude higher than that of a freshly deposited Ni film;[48] however, the exact mechanism of such an improvement has been in controversy for a long period. Boettcher *et al.* have evaluated the role of Fe in enhancing the activity of Ni-based OER electrocatalysts by electrochemical, *in situ* electrical, photoelectron spectroscopy and X-ray diffraction measurements,[32] and found that the addition of Fe not only improved the electrical conductivity of the NiFe composites but also, more importantly, modified the electronic properties of NiOOH by exerting a partial-charge-transfer activation effect on Ni, while this effect is commonly observed for other high-performance noble-metal electrode surfaces. In this case, based on the above discussion, we can attribute the performance enhancement of our NiFeOH@NF samples to the following factors: (i) the NiFeOH composites are inherently good catalysts for the OER; (ii) the reactive dip-coating method can *in situ* form the NiFeOH layer on the substrate with a binder-free manner, avoiding the subsequent deterioration of OER activity caused by the binder; (iii) the excellent electrical conductivity of the Ni foam substrate can facilitate the enhanced electron transfer for the more efficient electrocatalytic process; (iv) the rich structural defects in NiFe compounds can enable much more active sites for the catalytic reactions. At the same time, in order to examine the uniformity of the catalyst prepared with this method, a piece of Ni foam with a size of 100 × 30 mm was utilized to fabricate the NiFeOH electrode with the exact same procedure discussed above. The final NiFeOH-coated Ni foam was then cut into pieces with a size of 30 × 8 mm, while the OER activity of these pieces was independently measured with the CV plots depicted in Fig. S5.† It is found that all the different CV curves are very similar and the differences of the overpotential values are less than 5% under a current density of 50 mA cm^{-2}, implying the good uniformity of the catalysts prepared by this dip-coating method.

Previous reports showed that the Ni/Fe atomic ratio in the NiFe compounds can determine their catalytic performance towards the OER.[32,48] Here, the effects of the number of dip-coating times on the Fe/Ni atomic ratio of the NiFeO@NF

Table 1 The OER overpotential values for different catalysts assessed under different current densities in this work

j (mA cm^{-2})	η (mV)			j (mA cm^{-2})	η (mV)		
	NiFeOH@NF	Ni foam	Ruo_2		NiFeOH@NF	Ni foam	Ruo_2
1		267	227	100	249	—	326
10	210	374	275	150	258	—	347
20	218	394	262	200	266	—	—
50	234	—	301				

samples as well as on their OER activity were also studied. The SEM images of the NiFeO@NF samples prepared with 1, 2, 4 or 6 dip-coating times are shown in Fig. S6.† It is clear that when the number of dip-coating times increased, the surface of the samples became rougher and more flakes were generated. The corresponding EDS results (Table S5†) showed that the Fe/Ni atomic ratio was increased from 1/20.27 to 1/4.66 with the increasing number of dip-coating times, which implied more Fe content being introduced into the surface layer. However, this increasing number of dip-coating times did not yield any improvement in the OER catalysis and slight degradation in the OER activity was even observed by dip-coating 6 times (Fig. S7†). In regard of the above-mentioned results, one time of dip-coating was adopted to fabricate the NiFeO@NF samples in this work.

Furthermore, the ESCA of the electrode is another important parameter characterizing the efficient area involved in the electrode reaction. Here, the ESCA of Ni foams and NiFeOH@NF could be determined by measuring the non-faradaic electrical double-layer capacitance.[30] For the estimation of this surface area, a specific capacitance of $C_s = 0.040$ mF cm^{-2} in 1 M NaOH aqueous solution was employed for the assessment in 1 M KOH[30] and the results are shown in Fig. S8 and S9.† The ECSA of the bare NF and NiFeOH@NF were determined to be 11.26 and 15.94 cm^2, respectively. It is noted that an increment of about 1.4 times of the ESCA was obtained on NiFeOH@NF, which was consistent with the SEM result that the NF surface became much rougher after the dip-coating for the increased surface area and active sites for the enhanced OER activity. Also, ideal OER electrocatalysts not only hold excellent activity to drive water splitting but also a good stability in the long-duration of water electrolysis. The OER stability was then investigated by chronopotentiometry and illustrated in Fig. 5c. Under the current density of 50 mA cm^{-2}, a nearly constant operating potential could be kept at ~1.57 V (*i.e.* corresponding to an overpotential of 340 mV) for 50 hours in 1 M KOH. After the 50 hours of measurement, the CV plot did not demonstrate any noticeable degradation (Fig. 5d). Importantly, as illustrated in Fig. S10,† there was not any significant morphological changes after the measurement. All these results indicate that the NiFeOH@NF sample hold the excellent stability for the OER even under a high current density, which is advantageous for practical applications.

4. Conclusions

In conclusion, we have prepared the excellent NiFe-based OER eletrocatalysts by a facile reactive dip-coating method. This fabrication scheme is highly energy-saving, which only involves inexpensive equipment and regents as compared with other typical techniques. Importantly, the obtained catalysts of NiFeOH@NF can exhibit much better OER activity than that on commercial RuO_2 nanoparticles along with the impressive stability. Also, due to its easy implementation, low-cost and high-throughput, this dip-coating scheme can easily offer a feasible way for the scalable OER catalyst design for the sustainable production of clean chemical fuels from renewable energy resources. In future, such a reactive dip-coating method also can be used as a universal fabrication platform to prepare high-performance catalysts in large scale for different electrochemical or photoelectrochemical utilizations.

Acknowledgements

This research was supported by the General Research Fund of the Research Grants Council of Hong Kong SAR, China (CityU 11213115); the National Natural Science Foundation of China (Grant No. 51672229 and 51402160); the Science Technology and Innovation Committee of Shenzhen Municipality (Grant No. JCYJ20160229165240684); the Natural Science Foundation of Shandong Province (Grant No. ZR2014EMQ011); the Science and Technology Planning Project of Fujian Province (Grant No. 2014H2008); the Environment and Conservation Fund of Hong Kong SAR, China (ECF 2016-85); the City University of Hong Kong (Grant No. 9667124) and the Innovation and Technology Fund (Project No. ITS-380-14) from the Innovation and Technology Commission of the Government of the Hong Kong SAR.

References

1 A. Ursua, L. M. Gandia and P. Sanchis, *Proc. IEEE*, 2012, **100**, 410–426.
2 I. Dincer, *Int. J. Hydrogen Energy*, 2012, **37**, 1954–1971.
3 M. Carmo, D. L. Fritz, J. Mergel and D. Stolten, *Int. J. Hydrogen Energy*, 2013, **38**, 4901–4934.
4 L. Barreto, A. Makihira and K. Riahi, *Int. J. Hydrogen Energy*, 2003, **28**, 267–284.
5 I. C. Man, H. Su, F. Calle-Vallejo, H. A. Hansen, J. I. Martínez, N. G. Inoglu, J. Kitchin, T. F. Jaramillo, J. K. Nørskov and J. Rossmeisl, *ChemCatChem*, 2011, **3**, 1159–1165.
6 M. G. Walter, E. L. Warren, J. R. McKone, S. W. Boettcher, Q. Mi, E. A. Santori and N. S. Lewis, *Chem. Rev.*, 2010, **110**, 6446–6473.
7 M. E. G. Lyons and S. Floquet, *Phys. Chem. Chem. Phys.*, 2011, **13**, 5314–5335.
8 L. Han, S. Dong and E. Wang, *Adv. Mater.*, 2016, 1–26.
9 B. M. Hunter, H. B. Gray and A. M. Müller, *Chem. Rev.*, 2016, **116**, 14120–14136.
10 R. Subbaraman, D. Tripkovic, K.-C. Chang, D. Strmcnik, A. P. Paulikas, P. Hirunsit, M. Chan, J. Greeley, V. Stamenkovic and N. M. Markovic, *Nat. Mater.*, 2012, **11**, 550–557.
11 M. S. Burke, M. G. Kast, L. Trotochaud, A. M. Smith and S. W. Boettcher, *J. Am. Chem. Soc.*, 2015, **137**, 3638–3648.
12 A. J. Esswein, Y. Surendranath, S. Y. Reece and D. G. Nocera, *Energy Environ. Sci.*, 2011, **4**, 499–504.
13 S. Chen, J. Duan, Y. Tang, B. Jin and S. Zhang Qiao, *Nano Energy*, 2015, **11**, 11–18.
14 J. Xiao, Q. Lv, Y. Zhang, Z. Zhang and S. Wang, *RSC Adv.*, 2016, **6**, 107859–107864.
15 R. Gao, H. Zhang and D. Yan, *Nano Energy*, 2017, **31**, 90–95.
16 H. Liang, A. N. Gandi, D. H. Anjum, X. Wang, U. Schwingenschlögl and H. N. Alshareef, *Nano Lett.*, 2016, **16**, 7718–7725.

17 D. Das and K. K. Nanda, *Nano Energy*, 2016, **30**, 303–311.
18 L. Trotochaud, J. K. Ranney, K. N. Williams and S. W. Boettcher, *J. Am. Chem. Soc.*, 2012, **134**, 17253–17261.
19 M. Gong and H. Dai, *Nano Res.*, 2014, **8**, 23–39.
20 J. B. Gerken, S. E. Shaner, R. C. Masse, N. J. Porubsky and S. S. Stahl, *Energy Environ. Sci.*, 2014, **7**, 2376–2382.
21 X. Y. Lu and C. A. Zhao, *Nat. Commun.*, 2015, **6**, 6615.
22 Y. Yang, H. L. Fei, G. D. Ruan, C. S. Xiang and J. M. Tour, *ACS Nano*, 2014, **8**, 9518–9523.
23 W. J. Zhou, X. J. Wu, X. H. Cao, X. Huang, C. L. Tan, J. Tian, H. Liu, J. Y. Wang and H. Zhang, *Energy Environ. Sci.*, 2013, **6**, 2921–2924.
24 P. W. Menezes, A. Indra, C. Das, C. Walter, C. Göbel, V. Gutkin, D. Schmeiβer and M. Driess, *ACS Catal.*, 2016, 103–109.
25 H. F. Liang, F. Meng, M. Caban-Acevedo, L. S. Li, A. Forticaux, L. C. Xiu, Z. C. Wang and S. Jin, *Nano Lett.*, 2015, **15**, 1421–1427.
26 R. D. L. Smith, M. S. Prevot, R. D. Fagan, S. Trudel and C. P. Berlinguette, *J. Am. Chem. Soc.*, 2013, **135**, 11580–11586.
27 R. D. L. Smith, M. S. Prevot, R. D. Fagan, Z. P. Zhang, P. A. Sedach, M. K. J. Siu, S. Trudel and C. P. Berlinguette, *Science*, 2013, **340**, 60–63.
28 P. Ganesan, A. Sivanantham and S. Shanmugam, *J. Mater. Chem. A*, 2016, **4**, 16394–16402.
29 S. Zhao, Y. Wang, J. Dong, C.-T. He, H. Yin, P. An, K. Zhao, X. Zhang, C. Gao, L. Zhang, J. Lv, J. Wang, J. Zhang, A. M. Khattak, N. A. Khan, Z. Wei, J. Zhang, S. Liu, H. Zhao and Z. Tang, *Nat. Energy*, 2016, **1**, 16184.
30 C. C. L. McCrory, S. H. Jung, J. C. Peters and T. F. Jaramillo, *J. Am. Chem. Soc.*, 2013, **135**, 16977–16987.
31 J. D. Benck, Z. B. Chen, L. Y. Kuritzky, A. J. Forman and T. F. Jaramillo, *ACS Catal.*, 2012, **2**, 1916–1923.
32 L. Trotochaud, S. L. Young, J. K. Ranney and S. W. Boettcher, *J. Am. Chem. Soc.*, 2014, **136**, 6744–6753.
33 L. Liang, H. Cheng, F. Lei, J. Han, S. Gao, C. Wang, Y. Sun, S. Qamar, S. Wei and Y. Xie, *Angew. Chem., Int. Ed.*, 2015, **54**, 12004–12008.
34 J. Zhang, Y. Hu, D. Liu, Y. Yu and B. Zhang, *Adv. Sci.*, 2016, 1600343.
35 Y. Kuang, G. Feng, P. Li, Y. Bi, Y. Li and X. Sun, *Angew. Chem., Int. Ed.*, 2016, **55**, 693–697.
36 L. Marchetti, F. Miserque, S. Perrin and M. Pijolat, *Surf. Interface Anal.*, 2015, **47**, 632–642.
37 K. W. Park, J. H. Choi, B. K. Kwon, S. A. Lee, Y. E. Sung, H. Y. Ha, S. A. Hong, H. Kim and A. Wieckowski, *J. Phys. Chem. B*, 2002, **106**, 1869–1877.
38 J. Xiao and S. Yang, *J. Mater. Chem.*, 2012, **22**, 12253.
39 L. Qian, L. Gu, L. Yang, H. Yuan and D. Xiao, *Nanoscale*, 2013, **5**, 7388–7396.
40 T. Yamashita and P. Hayes, *Appl. Surf. Sci.*, 2008, **254**, 2441–2449.
41 T. Fujii, F. M. F. de Groot, G. A. Sawatzky, F. C. Voogt, T. Hibma and K. Okada, *Phys. Rev. B: Condens. Matter Mater. Phys.*, 1999, **59**, 3195–3202.
42 A. P. Grosvenor, B. A. Kobe, M. C. Biesinger and N. S. McIntyre, *Surf. Interface Anal.*, 2004, **36**, 1564–1574.
43 M. Aronniemi, J. Sainio and J. Lahtinen, *Surf. Sci.*, 2005, **578**, 108–123.
44 A. P. Grosvenor, B. A. Kobe and N. S. McIntyre, *Surf. Interface Anal.*, 2004, **36**, 1637–1641.
45 E. Fabbri, A. Habereder, K. Waltar, R. Kötz and T. J. Schmidt, *Catal. Sci. Technol.*, 2014, **4**, 3800–3821.
46 M. H. Miles, *J. Electroanal. Chem. Interfacial Electrochem.*, 1975, **60**, 89–96.
47 K. Zeng and D. Zhang, *Prog. Energy Combust. Sci.*, 2010, **36**, 307–326.
48 M. W. Louie and A. T. Bell, *J. Am. Chem. Soc.*, 2013, **135**, 12329–12337.